Published as: Maria T. Atanasova, Anastasia Vyalikh, Ulrich Scheler and Walter W. Focke. Characterization of rectorite from the Beatrix Gold Mine in South Africa. Accepted by Applied Clay Science Applied Clay Science Volume 126, June 2016, Pages 7–16 doi:10.1016/j.clay.2016.02.028 http://www.sciencedirect.com/science/article/pii/S0169131716300928

Characterization of rectorite from the Beatrix Gold Mine in South Africa

Maria T. Atanasova,[1,2] Anastasia Vyalikh,[3,4] Ulrich Scheler[3] and Walter W. Focke[2]

[1]Council for Geoscience, 280 Pretoria Street, Private Bag X112, Pretoria, South Africa. E-mail: mtg@geoscience.org.za

[2]Institute of Applied Materials, Department of Chemical Engineering, University of Pretoria, Private Bag X20, Hatfield 0028, South Africa. E-mail: walter.focke@up.ac.za

[3]Leibniz-Institut für Polymerforschung Dresden E.V., Hohe Strasse 6, 01069 Dresden, Germany

[4]Institut für Experimentelle Physik, Technische Universität Bergakademie Freiberg, 09596 Freiberg, Germany

Abstract

Three rectorite samples from the Beatrix Gold Mine, South Africa were characterized. Scanning electron microscopy revealed a layered morphology. High resolution transmission microscopy showed well distinguished light and dark layers of about 2.20 nm consistent with the 1:1 interstratified mica-smectite nature. X-ray diffraction measurements confirmed the basal spacing d_{001} of 2.20 nm consistent with a one-water-layer structure. Unit cell parameters, for a monoclinic unit cell with primitive lattice, refined to a = 5.177 Å; b = 8.980 Å; c = 22.489 Å and β = 97.335° with mean crystallite size around 14 nm and calculated cell volume of 1045 Å^3. The Greene-Kelly test suggested that the expandable smectite layers have montmorillonite-beidellite composition. Nuclear magnetic resonance spectroscopy indicated a high degree of Al substitution and the presence of two different Al sites corresponding to six- and four-fold octahedral and tetrahedral aluminum respectively. The chemical composition and diffraction data suggest that the mica is Na-Ca-rich, i.e. of paragonite-margarite series. The fixed interlayer regions (mica interlayers) contains proportionally dominant Na^+ and Ca^{2+} and minor amounts of K^+. The exchangeable smectitic interlayers contain almost equal amounts of Na^+ and Ca^{2+} ions. The distribution of the interlayer Na^+ ions was quantified by ^{23}Na solid-state NMR spectroscopy. It points to a three component mixed-layer structure with considerable variation in the composition of the mica layer of the different samples.

Keywords: Rectorite; Mixed-layer; Interstratification; XRD; SEM; solid-state NMR; Thermal analysis; FTIR.

1. Introduction

Rectorite is a 1:1 regular interstratification of dioctahedral mica and dioctahedral smectite (Bailey, 1981; Bailey et al., 1982; Brown, 1963). The swelling of the mineral is caused by the hydration of the exchangeable cations of the montmorillonite-like layers.

Rectorite occurrence of economic value exists in China (Hanlie et al., 2008). Rectorite was also discovered in the Beatrix Gold Mine located near Welkom, South Africa (von Rhaden, 1994). There it is found in modified shale bands, up to 0.5 m thick, both in the hanging and footwall of the Beatrix reef close to a major underground fault. The bands consist of low-grade metamorphic rock with mineral composition of quartz, muscovite, paragonite, chlorite, pyrophyllite, rectorite, smectite and chloritoid. The rectorite formation is associated with the alteration of other phyllosilicates, pre-existing pyrophyllite in particular, under metamorphic conditions of at least 350°C and 2.5 kbar (von Rhaden, 1994). The shale has been associated with gold losses at the mine in the process of physical and chemical extraction of the gold (Van Vuuren et al., 2000). Beatrix Mine rectorite is a Na-Ca-rich three-component mixed layer made up of smectite, paragonite and margarite (Jakobsen et al., 1995; Lausen, 1999).

The mixed-layer structure of rectorite, made up of alternating non-expandable (mica) and expandable (smectite) layers in a 1:1 ratio, defines a set of specific properties that differ from those of mica and smectite alone. For example rectorite dispersions provide for unique behavior, e.g. facilitating the synthesis of ultralight gels that are useful as adsorbents (Lu et al., 2015; Zheng et al., 2013). The present interest is in pursuing the use of this mixed-layer clay as nano-additive in polymer-based nanocomposites where it has also been found to impart desirable mechanical properties, e.g. improving the ductility of poly(lactic acid) (Li et al., 2009). This communication provides characterization data on Beatrix rectorite and is a first step towards this goal.

2. Materials and Methods

2.1. Materials

Three samples containing rectorite from Beatrix Mine were obtained and examined. Sample RT1 was collected in 1995, sample RT2 in 2010 and sample RT3 in 2012. The samples differ in their visual appearance with RT1 containing large light blue-grey platy aggregates with silky luster, while RT2 and RT3 represented disintegrated host rock mine material. All samples were subjected to various purification procedures aimed to produce high purity material for various tests and experimental applications. Unless otherwise indicated, the characterization presented in this paper is based on purified material with rectorite content above 90 wt.% (as determined by XRD analysis). Structurally and chemically the purified materials from the three samples were very similar and were categorized as rectorite, except where applicable specifics are highlighted.

2.2. Sample preparation

Sample preparation was applied as carefully as possible to prevent any physical distortion of the clay structure that may affect the experimental results. The general guidelines on sample preparation for clay minerals (Brindley and Brown, 1980; Moore and Reynolds, 1997) were followed with slight adaptations to accommodate specifics encountered in the preparation process.

Purification. Where applicable, the raw rectorite was first disaggregated with a laboratory jaw crusher (sample RT1) to break down large platy aggregates to around 1 to 2 mm, followed by further size reduction in a mixer-grinder. Samples RT2 and RT3 were sieved and the < 75 μm fraction used for further purification. Material (ca. 50 mg) was dispersed ultrasonically in deionized water (~250 mL) to allow disaggregation and the formation of a suspension. A settling time of 5 min was established for optimal recovery of

the clay fraction. The solid was separated from the water by centrifugation at 2000 rpm for 30 min. For oriented preparations, the clay residue, mixed with small amount of water, was deposited onto glass slides by a pipette and air-dried (AD) for XRD analysis. Glycerol (G) and ethylene glycol (EG) saturation was achieved by the vapor method. The AD oriented mounts were placed in a desiccator with glycerol or ethylene glycol for 16-18 h overnight at a temperature of 60°C and analyzed again on the X-ray diffractometer. The nature of the expandable component in the mixed-layer structure was determined by the Greene-Kelly test. It entails X-ray diffraction of Li-saturated oriented specimens after heating at 300°C followed by glycerol saturation (Greene-Kelly, 1952). The test was duplicated with high repeatability of the results. Relative humidity in the laboratory was maintained between 50% RH and 60% RH.

Removal of the calcium carbonate (12-15 wt.%) impurity from sample RT1 was accomplished by using 0.3 M acetic acid following a standard method (Ostrom, 1961). The separation was performed at room temperature and the process was closely watched by monitoring the pH after each cycle. The samples were repeatedly washed after effervescence had subsided. X-ray diffractograms were compared before and after exposure to acid to ensure that no damage to the rectorite structure had occurred.

Saturation of rectorite with various cations, i.e. lithium, sodium, potassium, strontium and barium, was achieved by treating about 20 g of sample with 1 M solution of the respective chlorides. The exchange procedure was carried out using a shaker for three days at room temperature. The frequency of the shaker was adjusted to 225 rpm. The saturation was repeated three times per day replacing the liquid each time with fresh solution containing an excess of the exchanging cation. The last round was completed by multiple washing with deionized water through three shaking sessions to remove excess chloride. To ensure that all chloride ions are removed a test was performed by reaction of an aliquot of

supernatant solution with 0.1 M $AgNO_3$. The washed clay was separated by centrifugation in acetone for 30 min at a speed of 2000 rpm.

Preparations for powder XRD (pXRD) measurements utilized a McCrone micronizing mill with corundum grinding elements. It reduced the mean particle size of the milled sample to ensure homogeneous subsample for X-ray diffraction. About 4 g of milled sample was ground with 10 mL ethanol for 8 min and each sample was prepared in duplicate. Calibration mixtures prepared by adding ZnO (or corundum) as an internal standard were ground and homogenized following the same procedure. Slurries were air dried and homogenized in a vibrating mill with steel balls prior to XRD measurements.

2.3. Characterization

Preliminary visual description and color imaging was done using a Leica Wild 10 binocular microscope. Morphological and structural observations and imaging were performed by scanning electron microscopy (SEM) and transmission electron microscopy (TEM).

The SEM/EDS analysis was carried out on a Leica Stereoscan 440 SEM linked to an OXFORD INCA EDS (Energy Dispersive System) using an acceleration voltage of 5 kV. The system is equipped with an Oxford X-Max SDD detector with 20 mm^2 active area and resolution of ca. 128 eV for Mn Kα (5895 eV). Examination was performed on polished specimens and grain mounts, coated with carbon for conductivity. High resolution imaging was obtained by ultrahigh resolution field emission SEM (HR FEGSEM Zeiss Ultra Plus 55) with an InLens detector at acceleration voltages of 0.6 kV to ensure maximum resolution of surface detail.

Transmission Electron Microscopy (TEM) imaging. A JEOL-JEM 2100F FETEM was utilized and operated at 100kV. Rectorite platelets were dispersed in ethanol using an ultrasound, deposited on Cu grid and left to air dry.

Nuclear magnetic resonance (NMR) spectroscopy. The purified rectorite samples were characterized by ^{1}H, ^{27}Al, ^{23}Na and ^{29}Si solid-state MAS NMR. All NMR measurements were performed on a 11.7 T Bruker Avance 500 spectrometer operating at the resonance frequencies of 500.13 MHz for ^{1}H, 130.34 MHz for ^{27}Al, 132.31 MHz for ^{23}Na and 99.36 MHz for ^{29}Si using a Bruker BL4 HXY 4 mm MAS and a BL 2.5 mm MAS probe-head. All spectra were fitted using Dmfit (Massiot et al., 2002).

^{27}Al MAS NMR spectra were acquired at a spinning frequency of 14 kHz. A single pulse of 2μs pulse duration ($<\pi/3$ for 30 kHz rf-amplitude) was applied to ensure a quantitative excitation of the central transition. High-power two-pulse phase modulation (TPPM) ^{1}H decoupling of 80 kHz rf field strength was applied. A recycle delay of 1 s and 256 repetitions were used. ^{27}Al chemical shifts were referenced externally to 1M $AlCl_3$ aqueous solution at 0 ppm.

The ^{29}Si solid state NMR spectra were acquired at a spinning frequency of 5 kHz with direct ^{29}Si polarization with ^{1}H decoupling (cw field strength 50 kHz), a single 90° pulse of 3 μs duration, recycle delays of 60 s (for higher signal-to-noise ratio) and 600 s (for a quantitative excitation) and 1024 repetitions. The ^{29}Si chemical shifts were referenced relative to TMS using Q8M8 as an external standard, which gives a $Si(-CH_3)_3$ signal at 12.6 ppm.

^{1}H MAS NMR spectra were measured at a recycle delay of 5 s employing a single 90° rf-pulse of 3 μs duration. The ^{1}H NMR spectra were referenced to TMS at 0 ppm using a NH_4 signal of ammonium dihydrogen phosphate at 6.7 ppm as an external reference.

For ^{23}Na MAS NMR measurements a single $\pi/2$ pulse of 2.5 μs was applied ensuring a quantitative excitation of the central transition. High-power two-pulse phase modulation (TPPM) ^{1}H decoupling of 80 kHz was applied. A recycle delay of 5 s and 2048 repetitions

were used. ^{23}Na chemical shifts were referenced externally to 1M NaCl aqueous solution at 0 ppm.

X-Ray Diffraction (XRD). X-ray data were recorded on a Bruker D8 Advance diffractometer with 2.2 kW Cu Kα radiation (λ=1.54060 nm), LynxEye detector with active area of 3.7° and Ni filter. The beam path included 0.2 mm (0.1°) Fixed Divergence Slit (FDS), 0.1 mm Receiving Slit (RS) and Soller slits of 2.5° on primary and secondary side. Scans from 2 to 70° 2θ for random powder preparations and 2 to 36° 2θ for oriented specimens were recorded in step scan mode at a speed of 0.02° 2θ steps size/5 s and generator settings of 40 kV and 40 mA. Sample spinner was on for all powder measurements for representative particle statistics. Rietveld refinements and quantification were done with DIFFRAC. TOPAS V4.2 software using the fundamental parameters approach (FPA) (Cheary and Coelho, 1992).

X-ray diffraction measurements were performed on oriented clay preparations, thin flakes of raw rectorite and random powder preparations. Diffraction data from oriented measurements at air-dried state and after various treatments were used to characterize the structure and swelling properties of rectorite. Random powder diffraction on micronized material was carried out to determine the nature and proportion of impurities. Details of the pXRD data analysis are presented in the Supplementary Material.

Chemical composition was determined by X-ray fluorescence (XRF) method. For major element analysis a milled sample (< 75 μm) of the neat, purified or exchanged material was roasted at 1000°C for at least 3 h to oxidize Fe^{2+} and S and to determine the loss of ignition (L.O.I.). Glass disks were prepared by fusing 1 g roasted sample and 8 g 12-22 flux consisting of 35 wt.% $LiBO_2$ and 64.71 wt.% $Li_2B_4O_7$ at 1050°C. For trace element analysis 12 g milled sample and 3 g Lico wax was mixed and pressed into a powder briquette by a hydraulic press with the applied pressure at 344 MPa. The glass disks and wax pellets were

analyzed by a PANalytical wavelength dispersive Axios X-ray fluorescence spectrometer equipped with a 4 kW Rh tube.

Fourier transform infrared spectroscopy (FTIR). Infrared spectra were recorded using a diamond ATR cell, which fitted in the macro sample compartment of a Bruker Optics Vertex 70v spectrometer. The sample compartment was evacuated during acquisitions and the contact area between the sample and the diamond ATR crystal was 2 mm in diameter. Spectra were recorded with 32 acquisitions at 4 cm^{-1} resolution over a spectral range of 4000-400 cm^{-1}.

Thermogravimetric analysis (TGA) was performed using the dynamic method on a Mettler Toledo A851 TGA/SDTA instrument. About 15 mg sample powder was placed in an open 70 µL alumina pan. Temperature was scanned from 25 to 1200°C at a rate of 10°C min^{-1} with air flowing rate of 50 mL min^{-1}.

3. Results

3.1. Microscopy

"Pure" rectorite from Beatrix mine features a platy-leafy morphology with a pale blue-grey color and brown pigmentation along cracks and folds, probably caused by iron contamination. Aggregates of stacked ultrafine flakes have a pearly luster with an earthy appearance and a soft soapy feel to the touch. Individual flakes are translucent to transparent (Figure 1) with thin, sharp edges. Scanning electron microscopy showed typical layered morphology. Platy and folded aggregates of compact parallel layers are either stacked continuously or thinly curled at the edges as shown in Figure 2. When immersed in water rectorite swells forming a viscous gelatinous mass.

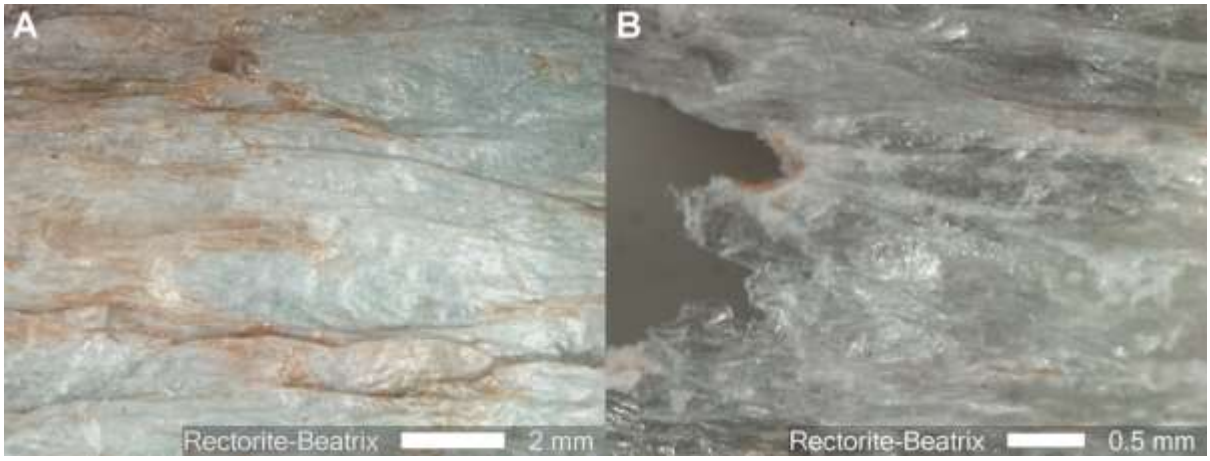

Figure 1. Binocular microscope photographs of Beatrix rectorite sample RT1. (A) Compact aggregate. (B) Translucent to transparent at sharp edges thin fragment (right)

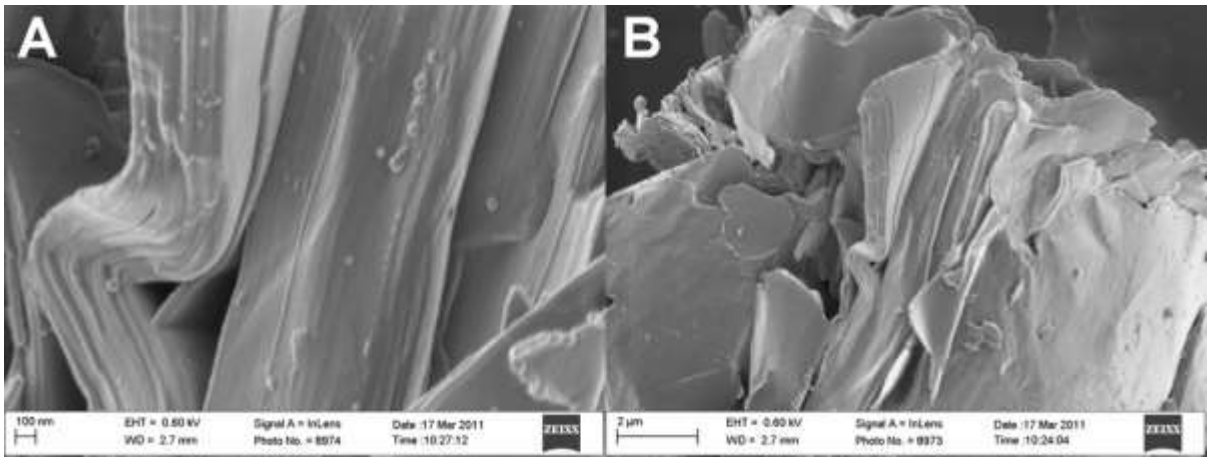

Figure 2. SEM images of platy folded and curled rectorite aggregates displaying typical layered textures (sample RT1).

Preliminary SEM observations of sample RT1 revealed calcite and quartz particles trapped between the rectorite sheets of larger platy rectorite fragments (Figure 3). In the disintegrated material from samples RT2 and RT3, rectorite coats individual quartz grains or serves as binding media for quartz and other impurities forming aggregates and lumps (Figure 4). This suggested that impurities could be liberated through ultrasonic dispersion and separated by gravity sedimentation. In this way it was possible to remove the larger-than-clay fraction components such as quartz. High resolution transmission microscopy (FETEM) performed on raw rectorite platelets shows continuous silicate layers in parallel to sub-

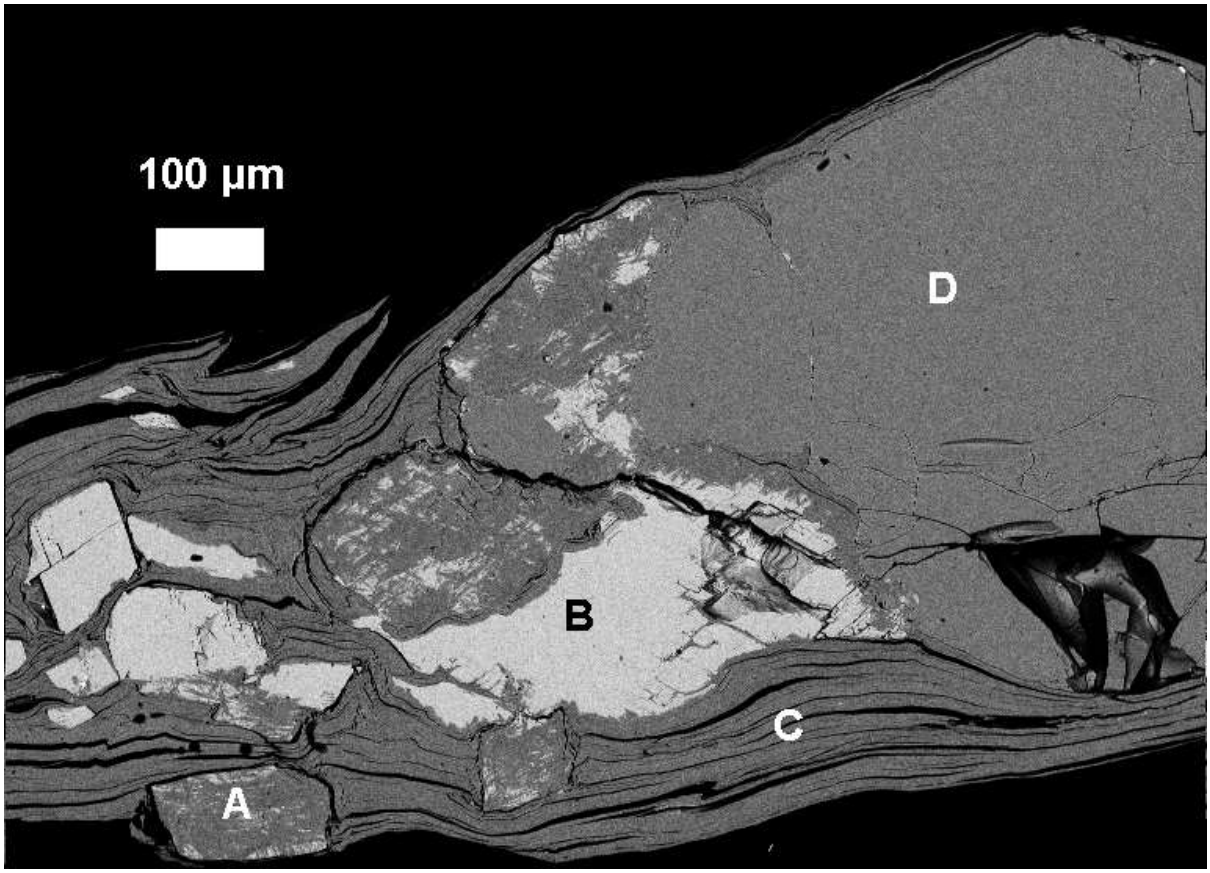

Figure 3. Low magnification SEM image of raw material from sample RT1 showing the distribution and relationship of (A) chlorite (light grey solid and finely mixed); (B) calcite; (C) rectorite (grey layered) with (D) quartz (grey solid).

parallel orientation. Ultra-thin edges display unambiguously regular periodicity of well-distinguished light and dark layers of about 2.0 nm and domains of higher thickness. Within the domains alternating contrast layers of spacing 1.00, 1.30 and 2.20 nm are visible at high magnification (Figure 5) identical with the basal spacing of mica and smectite or complete rectorite crystallite.

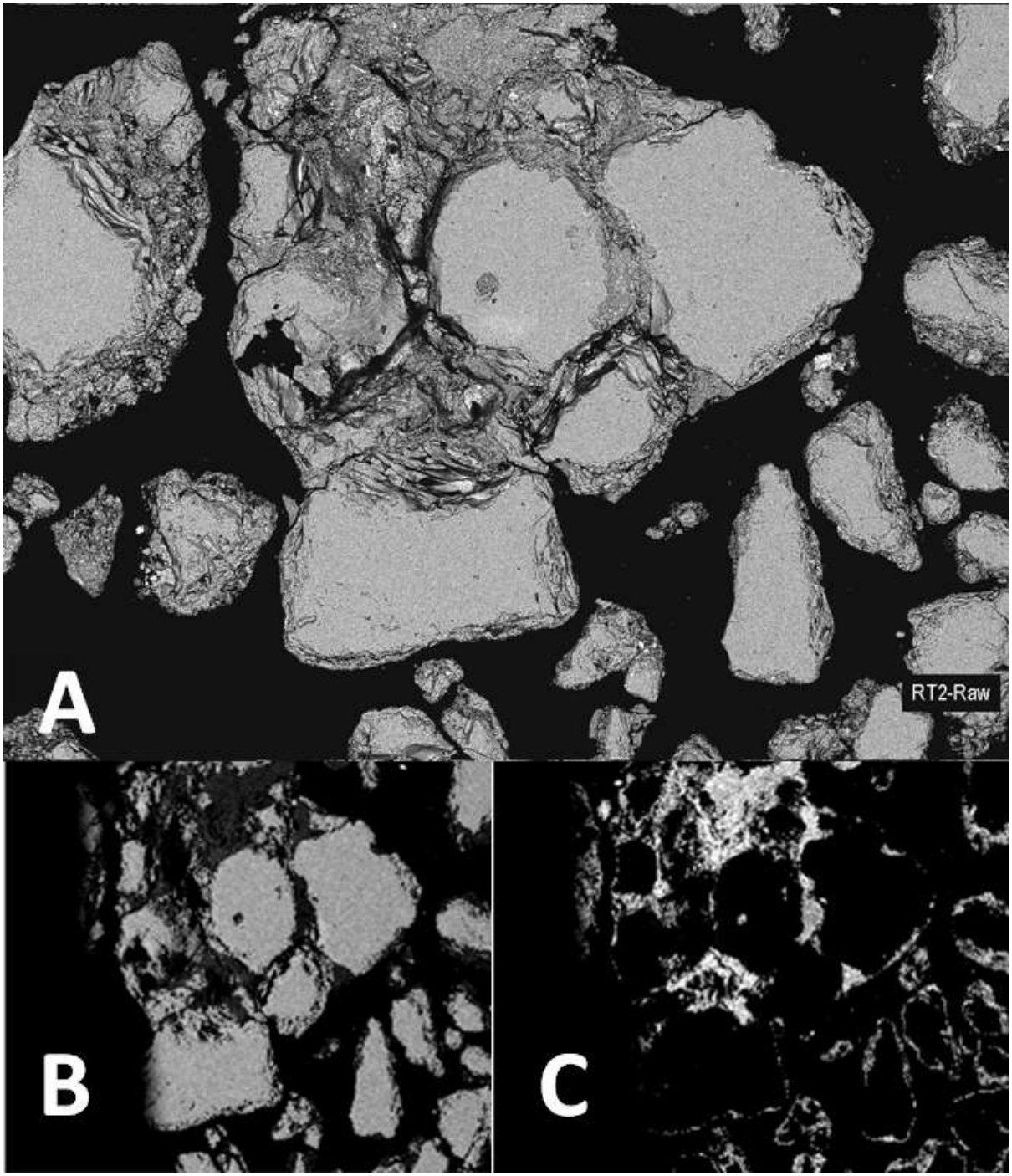

Figure 4. Low magnification backscatter electron (BE) SEM image (A), and element distribution maps for (B) Si and (C) Al from raw material (sample RT2) showing the natural occurrence and spatial relationship between rectorite, quartz and other minor impurities.

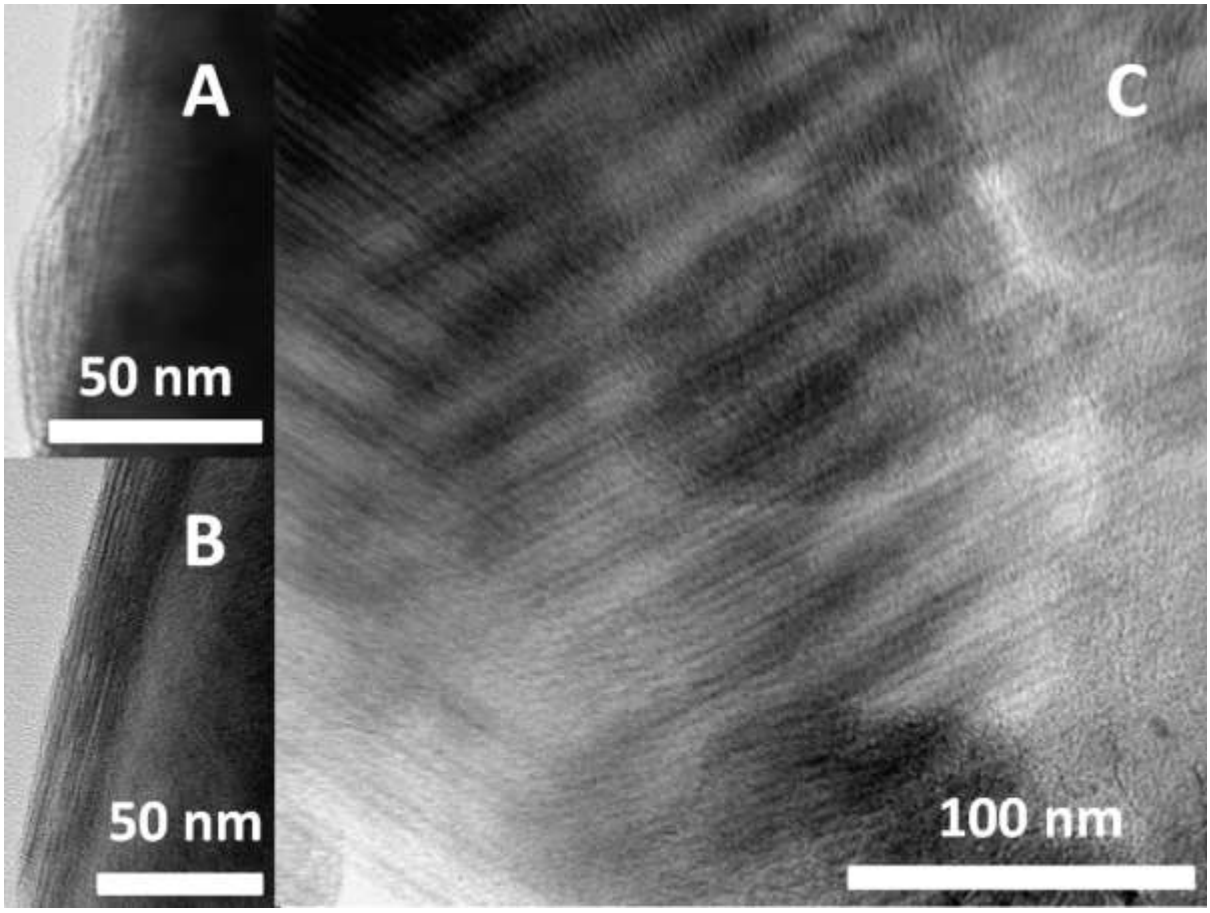

Figure 5. FETEM images of sample RT1 showing typical layer arrangement of rectorite. The thickness of light and dark domains is ~2.2 nm and higher. The spacing between the alternating contrast fringes within domains is ~1 to 1.3 nm and corresponds to the basal spacing of mica and smectite.

3.2. FTIR

Figure 6 shows the FTIR spectrum recorded for purified RT1. The IR vibration spectrum of untreated rectorite is in general agreement with published data for rectorite, montmorillonite and beidellite (Farmer, 1967; Kloprogge et al., 1999; Kodama, 1966; Madejová, 2001; Shimoda and Brydon, 1971). Although the spectrum of raw rectorite generally resembles a mixture of muscovite-paragonite and montmorillonite-beidellite spectra, it also contains unique bands and exhibits spectral sharpness not seen in either of the individual components or other interstratified clay mineral. Such bands at 1120 cm^{-1}, 993 cm^{-1} and 710 cm^{-1} are ascribed to Si-O stretching while the vibration at 925 cm^{-1} can be associated with the Al-OH

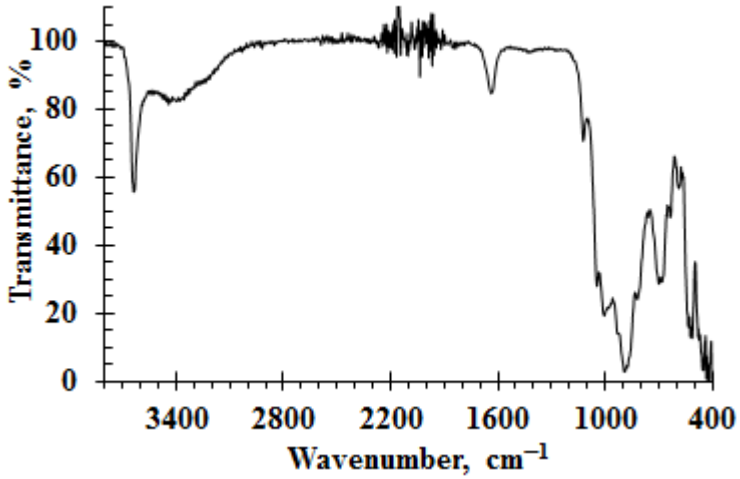

Figure 6. FTIR spectrum for purified rectorite (sample RT1).

deformation. Well-resolved sharp bands in the low frequency range from 450 cm^{-1} to 1200 cm^{-1} characteristic of phyllosilicate structure are present in both the raw and modified rectorite spectra. Apart from relatively minor shifts in peak positions, the modified forms feature considerable broadening of the absorption bands compared to those of neat sample. This is due to structural imperfections and reduced order arising from organic substitution. Two sharp bands at 1045 cm^{-1} and 1006 cm^{-1} assigned to Si-O-Si group are in close proximity to Si-O stretching in the tetrahedral sheet of beidellite at 1041 cm^{-1} and montmorillonite at 1010 cm^{-1} (Farmer, 1967). Two bands at 820 cm^{-1} and 698 cm^{-1} closely resemble Al-O out of plane vibrations in beidellite at 819 cm^{-1} and Si-O-Al bending at 693 cm^{-1}. These originate from Al for Si substitutions in the tetrahedral sheet of beidellite and are analogues to similar vibrations in muscovite (Farmer, 1967). The absorption peak at 892 cm^{-1} represents OH deformation band in either Al-OH-Al or Al (Fe^{3+})-OH groups described for Wyoming-type montmorillonite with high iron content (Russell, 1970) and results from the Fe^{3+} for Al^{3+} substitution in the octahedral sheet. However this vibration has also been reported for montmorillonites with very low iron content (Farmer, 1967) and could therefore also be ascribed to Al-OH band of rectorite. The OH absorption spectra in the high frequency

region above 3500 cm^{-1} are generally similar for raw and modified rectorite with slight broadening and intensity progressively decreasing from double to single chain surfactant intercalation. The sharp intense absorption band at 3638 cm^{-1} corresponds to structural H bonding vibrations in Si-O-Si linkage of rectorite (Kloprogge et al., 1999). Two less pronounced broad peaks at 3420 cm^{-1} and 1638 cm^{-1} are assigned to OH stretching and bending respectively in the H-O-H group of molecular water. The latter two are attributed to adsorbed and interlayer water molecules as both peaks disappeared upon heating at 200°C (Kodama, 1966). The band at 3638 cm^{-1} disappears at 900°C following complete dehydroxylation of the structure. Where a very weak and broad band appears in the spectra of raw samples at around 1375 cm^{-1}, it is due to trace amounts of adsorbed NH_4^+.

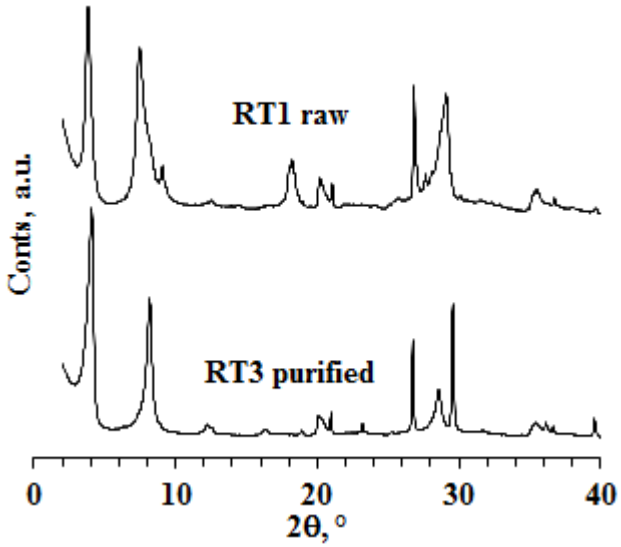

Figure 7. Powder diffraction patterns of a raw and a purified rectorite sample

3.3. XRD and thermal analyses

Typical pXRD diffractograms for a raw and highly purified sample are presented in Figure 7. Quantitative pXRD analysis (See the Supplementary Material) of bulk material from the three samples showed heterogeneous mineral assemblage with rectorite content between 58 wt.% and 75 wt.% associated with quartz (7-49 wt.%) and chlorite (1-6 wt.%) in all three

Table 4. XRD estimated proportions of rectorite and associated impurities in bulk and purified samples (wt.%).

Sample	**RT1**		**RT2**		**RT3**	
Phase	**Raw**	**Purified**	**Raw**	**Purified**	**Raw**	**Purified**
Rectorite	72.37(74)	91.27(33)	60.66(66)	86.32(65)	45.69(33)	91.45(71)
Quartz	7.78(19)	3.21(10)	28.83(45)	5.64(17)	48.81(20)	5.95(48)
Calcite	13.42(35)	0.66(15)	n.d.	n.d.	n.d.	n.d.
Muscovite	n.d.	n.d.	1.63(27)	2.93(35)	3.74(55)	1.66(20)
Chlorite	6.45(64)	4.86(30)	3.94(35)	2.44(47)	1.77(29)	1.52(27)
Pyrophyllite	n.d.	n.d.	3.40(37)	2.66(37)	n.d.	n.d.
Gypsum	n.d.	n.d.	1.55(14)	n.d.	n.d.	n.d.

samples; calcite (12-15 wt.%) in sample RT1; muscovite (1-4 wt.%) in samples RT2 and RT3 and pyrophyllite (2-4 wt.%) and gypsum (ca. 2 wt.%) detected only in sample RT2 (Table 4). Diffraction data of powdered raw rectorite obtained at room temperature and humidity showed fluctuation in basal spacing with average d_{001} values ranging from 22.00 Å to 23.73 Å within the three samples. Exposure to controlled 55% relative humidity (RH) in a desiccator showed that absorption of moisture is a function of time with largest expansion achieved after 90 h. The rectorite lattice expanded to 23.64 Å, 23.48 Å and 23.66 Å for RT1, RT2 and RT3 respectively.

Table 5. Major element concentrations of rectorite determined by X-ray fluorescence spectroscopy, recalculated for impurities concentrations compared to reported values (von Rhaden, 1994). The reported chemical compositions represent the mean values determinations based on five purified rectorite subsamples of RT3.

	Composition, wt.%		
Oxide	**Average**	**Recalculated***	**Literature#**
SiO_2	50.09 ± 0.38	49.56	51.02
TiO_2	0.27 ± 0.01	0.310	
Al_2O_3	37.57 ± 0.36	42.27	40.69
Fe_2O_3(t)	0.04 ± 0.02	0.049	0.40
MgO	0.01 ± 0.00	0.012	0.57
CaO	2.94 ± 0.07	3.388	5.33
Na_2O	2.81 ± 0.03	3.25	1.68
K_2O	0.95 ± 0.07	0.87	0.31
P_2O_5	0.02 ± 0.00	0.023	
Cr_2O_3	0.05 ± 0.05	0.058	
V_2O_5	0.02 ± 0.00	0.021	
BaO	0.05 ± 0.01	0.059	
ZnO	0.02 ± 0.01	0.024	
ZrO_2	0.01 ± 0.00	0.010	
SrO	0.08 ± 0.01	0.096	
L.O.I.	5.40 ± 0.04		
Dry basis	94.95 ± 0.61		
Total	100.14 ± 0.62		100.00

*Recalculated (ignited basis) adjusting for impurities based on the XRD mineral composition: rectorite 91.45 wt.%; quartz 5.95 wt.%, mica 1.66 wt.% and chlorite 1.52 wt.%. # Ignited-weight basis (von Rhaden, 1994)

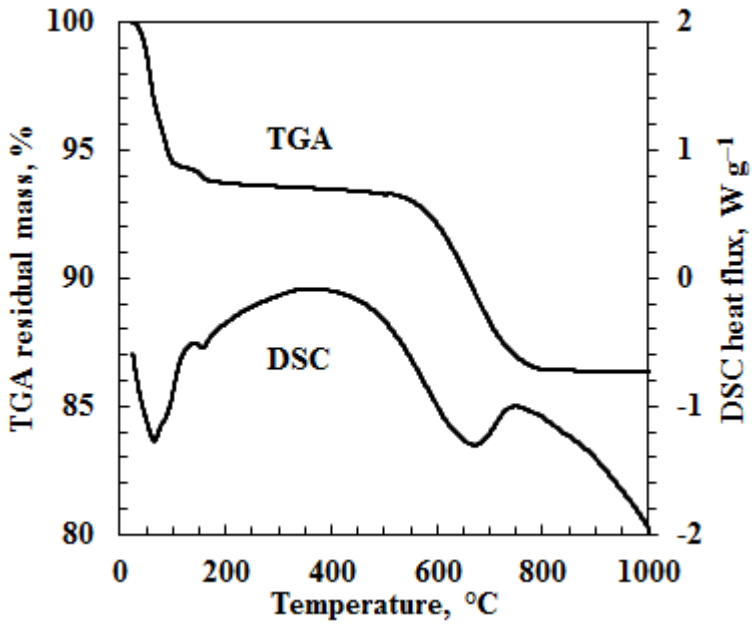

Figure 8. TGA/DSC curves for rectorite from the Beatrix mine recorded at a scan rate of 10°C min^{-1} with air flowing at 30 mL min^{-1}. The sample was equilibrated at 55% relative humidity (RH) in a desiccator for more than 90 h.

The results of TGA/DSC thermal analysis (Figure 8) supplemented by X-ray diffraction examination of heated specimens demonstrate the response of rectorite to heating. Overlays of XRD diffractograms recorded from rectorite specimens heated to 1200°C in steps of 50°C are presented in Figure 9. The two methods generally agreed that full decomposition of rectorite occurred in three major steps with total weight loss of 15.2%

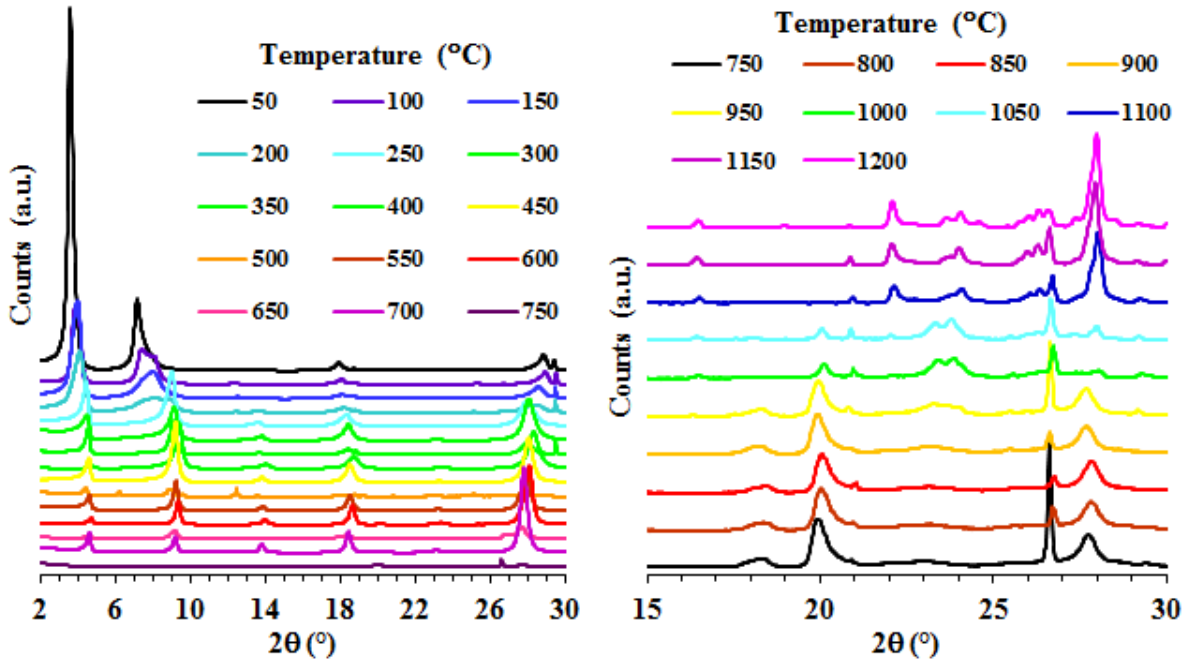

Figure 9. Overlay of X-ray diffraction patterns of rectorite heated at 50°C intervals: Temperature range 50°C to 1200°C.

(Figure 8). A fast steep drop below 150°C is followed by slow and continuous mass loss between 200 and 470°C and a significant decrease in mass between 470 to 800°C (Figure 8). Gradual displacement of basal XRD lines with dehydration accompanied by asymmetric broadening and overall decrease in intensity profiles at low angles evidence the structural transformations in response to elevating temperatures. Initially the structure slightly expands between 50°C to 100°C, possibly due to steam formation in the interlayer region on heating. At the start 50°C to 100°C basal reflections fluctuate with d_{001} from 22.20 Å through 22.37 Å to 23.29 Å and back to initial 22.29 Å at 150°C - 200°C. The DSC patterns feature three endothermic peaks at 53°C, 73°C and 140°C associated with progressive TGA mass loss of 5.9 wt.% completed at 150°C. This mass loss is consistent with desorption of surface water and loss of the interlayer water (Kodama, 1966). The two endothermic peaks at low temperatures indicate dehydration from smectite layer with divalent cation, i.e. beidellite where Ca^{2+} is the interlayer cation (Hendricks et al., 1940). The IR spectra support this

observation by the disappearance of OH stretching bands at 3420 cm^{-1} and 1640 cm^{-1}. A downshift and significant intensity drop of d_{001} to 19.79 Å accompanied by increased d_{002} now at 9.89 Å marks the loss of regularity and collapse of the clay structure at 250°C. Further increase in temperature results in change of profile intensity ratios, i.e. a very weak 001, enhancement of intensity around the mica region and adjusting positions to those consistent with paragonite d_{002} at 9.65 Å, d_{004} at 4.80 Å and d_{006} at 3.20 Å around 450°C - 500°C. From this point up to around 750°C the 001 reflection is very weak and gradually disappears. The loss of intensity at the first basal reflection indicates the end of dehydroxylation with the complete breakdown of the interlayer, i.e. the periodicity along c-direction has seized to exist. On the TG/DSC plots a week broad peak at around 470°C and a more intense one at 715°C are attributed to dehydroxylation. At 950°C formation of mullite commences, followed by cristobalite at 1050°C and albite at 1100°C. By 1000°C the clay structure is completely destroyed. The TGA curve indicated a mass loss of 7.7 wt.% between 500°C to 820°C related to dehydroxylation of structural hydroxyl groups.

3.4. NMR

NMR probes the local environment of the nucleus under study and thus it is focusing on the short-range order. NMR probes the local environment of the nucleus under study, it therefore is ideally suited for disordered materials or materials exhibiting short-range order only. The NMR spectra provide quantitative information complementary to the scattering experiments on the relative content of various species. NMR inherently gives an ensemble average. Therefore solid-state NMR spectra of all NMR-active nuclei in the sample were recorded.

^{27}Al MAS NMR. ^{27}Al MAS (14 kHz) NMR spectra of all samples showed two signals with spinning side-bands (ssb) (Figure 10 (a) and (b)). The central transitions of the lines featured characteristic second-order quadrupolar broadened line shapes. The dominating

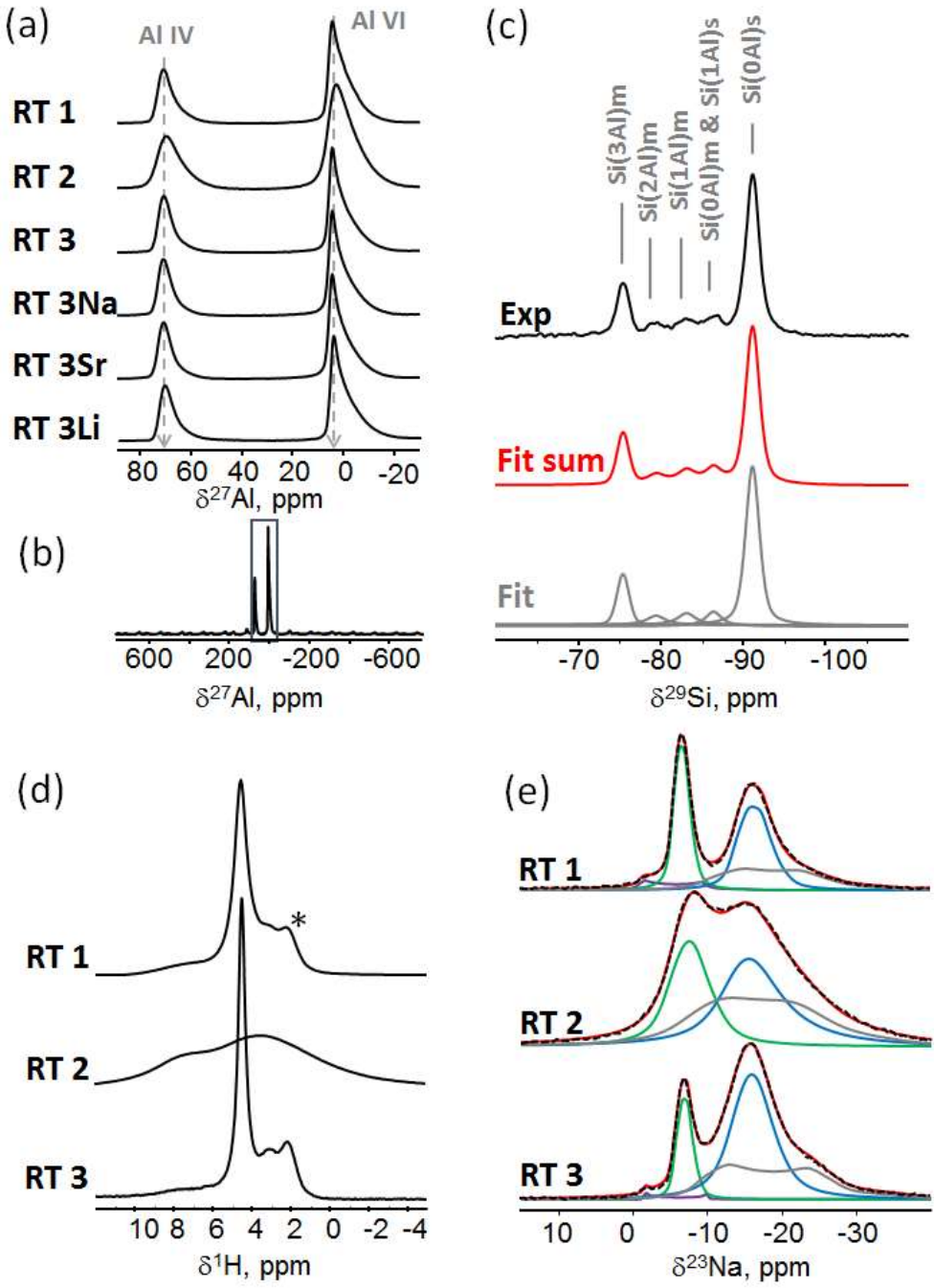

Figure 10. (a) ^{27}Al MAS NMR spectra of rectorite samples, (b) broad width ^{27}Al MAS NMR spectrum of RT1 with spinning sidebands. Frame shows the spectral region expanded in (a). (c) ^{29}Si MAS NMR spectrum of RT1 (Exp) with spectral deconvolution (Fit) and a sum of fit components (Fit sum). (d) ^{1}H MAS NMR spectra at 20 kHz spinning speed of the three rectorite samples. The spectra are normalized at the high-field peak shown by asterisk. (e) ^{23}Na MAS NMR spectra of the three rectorite materials (black dotted lines) with their deconvolution including the sum of fit components (red line). Site I is green, Site II is grey, Site III is blue and Site IV is lilac.

line at *ca.* 5 ppm is attributed to six-coordinated (or octahedral or AlO_6 or Al-VI) Al site, while the second peak at ca. 70 ppm is known to arise from Al sites in the tetrahedral coordination (four-coordinated AlO_4 or Al-IV) (Vyalikh et al., 2009). The relative ratio of AlO_4 (Al-IV) to AlO_6 (Al-VI) is 1:2 and remained constant across all samples. Deviation from the characteristic second-order quadrupolar lineshape due to inhomogeneous broadening indicates a distribution of Al environments. The fit parameters changed only slightly within the uncertainty limits, pointing to the fact that the local structure around Al was not affected by purification and ion substitutions. Similar spectral parameters and the invariance of the ^{27}Al NMR spectra on modification of the local environment in interlayers were previously reported for synthetic beidellite (Kloprogge et al., 1992). Slight deviations of the fit parameters for RT2 and its remarkable line broadening reflects a more disordered and less symmetric environment as compared to other samples (Table 1).

Table 1. Fit data for ^{27}Al NMR spectra, where $^{27}\delta$ is isotropic chemical shift (±0.2 ppm) and C_Q is quadrupolar coupling constant (±0.2 MHz). Relative intensities (±1%) for two components are calculated from central transitions and spinning side bands.

Sample	$^{27}\delta$, ppm		C_Q, MHz		Relative intensities, %	
	Al-IV	Al-VI	Al-IV	Al-VI	Al-IV	Al-VI
RT1	74.3	6.6	3.4	3.6	33	67
RT2	74.5	6.8	4.0	4.2	32	68
RT3	74.0	6.5	3.1	3.5	33	67
RT3 Na	74.2	6.6	3.2	3.5	33	67
RT3 Sr	74.2	6.6	3.2	3.5	33	67
RT3 Li	74.1	6.5	3.3	3.6	33	67

^{29}Si MAS (5 kHz) NMR. Since T_1 relaxation times can be different for various ^{29}Si sites, the repetition time had to be adjusted according to the longest T_1 in the sample in order to obtain quantitative spectra. Due to the very long ^{29}Si T_1 relaxation times in these materials ^{29}Si MAS NMR spectra were measured at two repetition time values in order (*i*) to obtain a sufficient signal-to-noise ratio for signal assignment and (*ii*) to obtain quantitative information from fully relaxed spectra. Five lines are found in all ^{29}Si spectra, which are attributed to silicon tetrahedra surrounded by aluminum atoms located in either the mica (m) or the smectite (s) layers (Figure 10 (c)). The nomenclature Si(*n*Al) designates a Si atom bonded via oxygen bridges to *n* Al atoms in tetrahedral sheets (*n* = 0-3). Due to their similar positions $Si(0Al)_m$ and $Si(1Al)_s$ cannot be distinguished in the present experiment. The Si(*n*Al) intensity distribution presented in Table 2 shows a deviation from the expected binomial intensity distribution in mica pointing to a high degree of Al substitution (high fraction of the $Si(3Al)_m$ component).

Table 2. Fit data for ^{29}Si NMR spectra, where $^{29}\delta$ is isotropic chemical shift (±0.1 ppm). Relative intensities (±5%) are calculated from the fully relaxed spectra (at a repetition time of 600 s).

Sample	**^{29}Si chemical shifts**					**Relative**
RT1	−75.5	−79.5	−83.2	−86.3	−91.1	20 : 6 :
RT3	−75.5	−79.5	−82.7	−86.7	−91.0	13 : 10 :
RT3 Na	−75.5	−79.3	−82.8	−85.7	−91.0	11 : 8 : 1
RT3 Sr	−75.5	−79.3	−83.6	−86.3	−91.1	12 : 12 :
RT3 Li	−75.5	−79.3	−83.2	−86.1	−91.0	11 : 13: 1
Assignment	**Si(3Al)m**	**Si(2Al)m**	**Si(1Al)m**	**Si(0Al)m Si(1Al)s**	**Si(0Al)s**	

^{1}H MAS (20 kHz) NMR. High-resolution MAS NMR spectra (Figure 10(d)) show sharp signals at 2.1 ppm, 3.1 ppm, and 4.6 ppm and a broad background signal at ca. 8 ppm for the samples RT1 and RT3, while only two broad peaks are seen for RT2. The broadening can arise from structural disorder and/or the presence of minor paramagnetic impurities (for example, the presence of iron oxide or iron substitution in the octahedral sheets of the rectorite itself) and is consistent with the ^{27}Al and ^{23}Na data for RT2. The peaks at 2.1 ppm and 3.1 ppm are assigned to the hydroxide groups of hydrated Al_2O_3 and SiO_2 in the mineral structure, while the peak at 4.6 ppm is attributed to water physically adsorbed on the mineral surface. Similar peaks have been noted in a study on aluminum layered hydroxides (Wang et al., 2009). In contrast with this study (Wang et al., 2009), the narrower linewidth and Lorentzian lineshape in the present study point to weak residual dipolar interactions and thus higher mobility of water, because the proton dipolar coupling is the major source of broadening. The broad peak at ca. 8 ppm can arise from interlayer water surrounding the Na^+ in the interlayer space of the smectite layers. In general, the presence of water and hydroxide signals are in a good agreement with the FTIR data reported above.

^{23}Na MAS (20 kHz) NMR. The ^{23}Na NMR spectra of RT1 and RT3 exhibit at least three major components, while in the spectrum of RT2, only two components are resolved due to the very strong line broadening (Figure 10(e)). The well resolved signal at the low-field side (positive ppm values) characterized by a $\delta(^{23}Na)$ value of ca. −5 ppm, a C_Q value of 1 MHz, η of 0.5 and narrow line broadening is attributed to Na^+ fixed in between margarite tetrahedral sheets according to the literature data (Site I, green line in Figure 10(e)) (Jakobsen et al., 1995). Deviations in both $\delta(^{23}Na)$ and C_Q for RT2 point to changes in the local electron environment around the sodium atom in RT2 margarite sheets, while the increase of its linewidth (EM) indicates greater disorder in comparison to the other samples.

The high-field broad line represents a superposition of the components with more pronounced quadrupolar characteristic, in which the strength and distribution of quadrupolar interactions point to symmetry and ordering in the local sodium environment. Site II at ca. $\delta(^{23}Na) = -7$ ppm possesses a large C_Q of ca. 2.8 MHz (grey line in Figure 10(e)), indicating even larger deviations from the spherical symmetry around a sodium atom in RT2 and RT3. The higher EM value informs about structural inhomogeneity and disorder, which has been significantly improved in Sample RT3. Site III (blue line in Figure 10(e)) is characterized, in general, by a $\delta(^{23}Na)$ value of ca. -13 ppm and a C_Q value of 1.2 to 1.5 MHz. According to the data reported for Beatrix rectorite (Jakobsen et al., 1995), the high-field broad line giving rise to Sites II and III, may results from overlap between Na^+ fixed between paragonite tetrahedral sheets and exchangeable Na^+. In addition, a very weak signal (lilac line in Figure 10(e) at ca. 1 ppm and a C_Q of 2.2 MHz (up to 5% of total intensity) is visible in RT1 and RT3. In literature, the narrow ^{23}Na peak at ca. 0 ppm is attributed to trapped Na^+ ions in symmetric cavities created by a mica-type stacking or to nonexchangeable part of the sodium interlayer cations (Möller et al., 2010). In contrast to that work, the quadrupolar interactions for this peak

are not averaged out, and it can tentatively be assigned to a variety of Na-containing mica in the samples under study. Although for accurate assignment additional experiments are required, the assumption is that Site III with smaller quadrupole parameters results from more mobile exchangeable Na^+ in smectitic interlayer. This allows to estimate the ratio of Na^+ fixed between margarite and paragonite tetrahedral sheets, which is found to be 1:0.8, 1:1.4 and 1:2.2 for RT1, RT2 and RT3, respectively. Exact quantification for RT2 is impossible at this stage due to strong signal overlapping. The effect of interlayer composition on the

distribution of Na^+ for various exchanged forms of rectorite is beyond the scope of the present study.

In summary, the NMR results indicate that two Al sites are present in all rectorites (Al-VI and Al-IV). The local structure around Al does not vary upon modification and a high degree of Al substitution is indicated. Structural inhomogeneity and disorder are indicated for RT2 rectorite. The relative concentrations of Na^+ fixed between margarite and paragonite differ in the three rectorite samples.

3.5. XRF

Average chemical composition of purified rectorite (RT3) determined by XRF analysis is listed in Table 5. Those with the highest rectorite content were recalculated adjusting for mineral impurities and used as basis to calculate the mean structural formula. Trace concentrations of P_2O_5, Cr_2O_3, ZnO and BaO were considered matrix contamination and omitted from further calculations. The CEC, estimated from the XRF-determined compositions of the purified and the various RT3 cation exchanged samples, was 45 ± 7 mEq/100 g. Such a value is expected if alternate interlayers are of the montmorillonite type. The compositions of the fixed and exchangeable interlayers were determined from Na^+ and K^+ cation exchanged rectorite forms under the assumption that all exchangeable cations reside in the swelling interlayer region. The exchangeable interlayer composition is ($Na_{0.10}$ $Ca_{0.13}$) with layer charge of −0.36 per $O_{20}(OH)_4$ and the fixed interlayer contains ($Na_{0.66}$ $Ca_{0.31}K_{0.13}$) with total charge of −1.41. The summarized formula derived from ignited composition (dry basis) based on $O_{20}(OH)_4$ is:

$$(Na_{0.76}\,Ca_{0.44}K_{0.13})[Al_{4.03}Ti_{0.03}(Fe,Mg)_{0.006}](Si_6Al_2)O_{20}(OH)_4.nH_2O \quad (1)$$

The structural formula indicates that monovalent Na^{+}, K^{+} and divalent Ca^{2+} cations are available in the interlayer of natural rectorite. The fixed interlayer space (mica interlayer space) contains proportionally dominant Na^{+} and Ca^{2+} and minor K^{+}. The exchangeable smectitic interlayer contains almost equal Na^{+} and Ca^{2+} ions. This elemental distribution implies that the mica layer is represented by paragonite (Na-mica)-margarite (Ca-mica with minor Na) series, rather than muscovite (K-mica). Furthermore, this composition suggests a 1:2.5 margarite to paragonite distribution. This agrees well with the margarite to paragonite distribution of 1:2.2 in RT3 estimated from the ^{23}Na NMR data. The expandable layer charge of −0.36 is predominantly due to tetrahedral substitution characteristic of beidellite rather than montmorillonite where the net layer charge arises from octahedral substitutions. In the dioctahedral 2:1 structure the four octahedral sites are dominantly occupied by Al^{3+} with minor Ti^{4+}, Fe^{3+} and Mg^{2+}. Based on chemical data distribution of tetrahedral and octahedral Al is proportionally 1:2. These conclusions support the XRD identification of beidellite by the Greene-Kelly test (Greene-Kelly, 1952); identification of paragonite by thickness of the mica layer of 9.65 Å as opposed to muscovite of 10.00 Å. Hence, Beatrix rectorite identifies with Na-Ca-rectorite and that conform well to previously reported data for rectorite from this locality (Jakobsen et al., 1995; von Rhaden, 1994).

Smectites and other 2:1 layered structures commonly exhibit heterogeneous charge distribution among the different layers (Lagaly and Beneke, 1991). In mixed layer structures heterogeneity is further emphasized by the existence of two types of 2:1 layers. The structural formulae therefore, derived from major element concentrations as above represent average compositions of the layers.

4. Conclusions

Based on major element concentrations, X-ray diffraction and NMR evidence, rectorite from Beatrix mine identifies with Na-Ca-rectorite, a dioctahedral regular interstratification of mica-smectite type. The dioctahedral character of the interstratified structure was confirmed by d_{060} at 1.48 Å. There are Na^{+}, Ca^{2+} and K^{+} cations in the fixed interlayer region (mica interlayer) in approximately 15:7:3 ratio and the cationic presence of the exchangeable smectitic interlayer comprises Na^{+} and Ca^{2+} ions in about a 3:4 ratio. These compositions indicate that the mica layer is represented by paragonite (Na-mica)-margarite (Ca-mica) series, rather than muscovite (K-mica). The structural formula also indicates relatively high tetrahedral substitution resulting in expandable layer charge of −0.36 characteristic of beidellite rather than montmorillonite where the net layer charge arise from octahedral substitutions. Furthermore, the chemical data and derived structural formula of Beatrix rectorite suggest an Al-IV:Al-VI ratio of 1:2. The four octahedral sites are dominantly occupied by Al^{3+} with minor Ti^{4+}, Fe^{3+} and Mg^{2+}. Variable interlayer composition of the mica component amongst the samples is indicated by NMR and chemically by XRF data.

These conclusions are supported by the NMR and XRD findings discussed above and conform to previous reports of paragonite-margarite type mica layers alternating Na-montmorillonite-beidellite swelling component in rectorite from this locality (Jakobsen et al., 1995). Additionally, the ^{1}H MAS (20 kHz) NMR data reported in this work contributes to the understanding of the nature and position of the metal hydroxide groups in the mineral structure and physically adsorbed water and metal bound OH-groups in the rectorite studied here. A previous study on aluminum layered hydroxides (Wang et al., 2009) reported similar peak positions, however peak characteristics observed in the present work point to weak residual dipolar interactions and thus higher mobility of water.

Although the bulk “in-situ” occurrence of rectorite in the three samples from Beatrix Mine shows rather heterogeneous mineral associations and physical appearance,

mineralogically, structurally and chemically all the purified rectorite samples are identified as Na-Ca-rectorite. Thus the Beatrix rectorite appears to be compositionally different from the (K, Na, Ca)-rectorite from the Zhongxiang deposit in Hubei, China (Hanlie et al., 2008), the Na-rich rectorite from Arkansas, USA (Jakobsen et al., 1995) and the (Na, K, Mg, Ca, Sr)-rectorite specimens from Baluchistan, Pakistan (Kodama, 1966).

Acknowledgments

Financial support for this research from the Algeria/South Africa Collaboration Programme of the National Research Foundation (NRF) is gratefully acknowledged. The authors are indebted to the Council for Geoscience, the University of Pretoria, South Africa and the Leibniz-Institut für Polymerforschung Dresden e.V. and the Institut für Experimentelle Physik, Technische Universität Bergakademie Freiberg, Germany for technical support and for making instrumentation available for this research.

References

Bailey, S.W., 1981. A system of nomenclature for regular interstratifications. Canadian Mineralogist 19, 651-655.

Bailey, S.W., Brindley, G.W., Kodama, H., Martin, R.T., 1982. Report of the Clay Minerals Society Nomenclature Committee for 1980-1981. Clays & Clay Minerals 30, 76-78.

Brindley, G.W., Brown, G., 1980. Crystal structures of clay minerals and their X-ray identification (Mineralogical Society Monograph No.5), Mineralogical Society, London.

Brown, G., Weir, A.H., 1963. The identity of rectorite and allevardite, in: Rosenquist, T., Graff-Petersen, P. (Ed.), Int. Clay Conf., Pergamon Press, Stockholm, pp. 27-35.

Cheary, R.W., Coelho, A., 1992. Fundamental parameters approach to X-ray line-profile fitting. Journal of Applied Crystallography 25, 109-121.

Farmer, V.C., Russel, J.D., 1967. Infrared absorption spectroscopy in clay studies: Vibrations of the hydroxyl group. Clays and Clay Minerals 15, 121-141.

Greene-Kelly, R., 1952. A test for montmorillonite. Nature 170, 1130-1131.

Hanlie, H., Xiaoling, Z., Miao, W., Yijun, H., Dengwen, D., 2008. Morphological characteristics of (K, Na)-rectorite from Zhongxiang rectorite deposit, Hubei, Central China. Journal of China University of Geosciences 19, 38-46.

Hendricks, S.B., Nelson, R.A., Alexander, L.T., 1940. Hydration mechanism of the clay mineral montmorillonite saturated with various cations. Journal of the American Chemical Society 62, 1457-1464.

Jakobsen, H.J., Nielsen, N.C., Lindgreen, H., 1995. Sequences of charged sheets in rectorite. American Mineralogist 80, 247-252.

Kloprogge, J.T., Frost, R.L., Hickey, L., 1999. Infrared absorption and emission study of synthetic mica-montmorillonite in comparison to rectorite, beidellite and paragonite. Journal of Materials Science Letters 18, 1921-1923.

Kloprogge, J.T., Jansen, J.B.H., Schuiling, R.D., Geus, J.W., 1992. The interlayer collapse during dehydration of synthetic $Na_{0.7}$-Beidellite: A ^{23}Na solid-state magic-angle spinning NMR study. Clays and Clay Minerals 40, 561-566.

Kodama, H., 1966. The nature of the component layers in rectorite. American Mineralogist 51, 1035-1055.

Lagaly, G., Beneke, K., 1991. Intercalation and exchange reactions of clay minerals and non-clay layer compounds. Colloid & Polymer Science 269, 1198-1211.

Lausen, H., Lindgreen, H., Jakobsen, H.J., Nielsen, N.C., 1999. Solid-state 29 Si MAS NMR studies of illite and illite-smectite from shale. American Mineralogist 84, 1433-1438.

Li, B., Dong, F.X., Wang, X.L., Yang, J., Wang, D.Y., Wang, Y.Z., 2009. Organically modified rectorite toughened poly(lactic acid): Nanostructures, crystallization and mechanical properties. European Polymer Journal 45, 2996-3003.

Lu, Y., Chang, P.R., Zheng, P., Ma, X., 2015. Porous 3D network rectorite/chitosan gels: Preparation and adsorption properties. Applied Clay Science 107, 21-27.

Madejová, J.K., P., 2001. Baseline studies of the clay minerals society source clays: Infrared methods. Clays and Clay Minerals 49, 410-432.

Massiot, D., Fayon, F., Capron, M., King, I., LeCalve, S., Alonso, B., Durand, J.-O., Bujoli, B., Gan, Z., Hoatson, G., 2002. Modelling one- and two-dimensional solid-state NMR spectra. Magnetic Resonance in Chemistry 40, 70-76.

Möller, M.W., Hirsemann, D., Haarmann, F., Senker, J., Breu, J., 2010. Facile scalable synthesis of rectorites. Chemistry of Materials 22, 186-196.

Moore, D.M., Reynolds, R.C., 1997. X-ray Diffraction and the Identification and Analysis of Clay Minerals, 2 ed. Oxford University Press, New York.

Ostrom, M.E., 1961. Separation of clay minerals from carbonate rocks by using acid. Journal of Sedimentary Research 31, 123-129.

Russell, J.D., Farmer, V.C. Velde, B., 1970. Replacement of OH by OD in layer silicates, and identification of the vibrations of these groups in infra-red spectra. Mineralogical Magazine 37, 869-879.

Shimoda, S., Brydon, J.E., 1971. I.R. studies of some interstratified minerals of mica and montmorillonite. Clays and Clay Minerals 19, 61-66.

Van Vuuren, C.P.J., Snyman, C.P., Boshoff, A.J., 2000. Gold losses from cyanide solutions. Part I: The influence of the silicate minerals. Minerals Engineering 13, 823-830.

von Rhaden, H.V.R., 1994. Rectorite: A new phyllosilicate species in Witwatersrand palaeoplacers. Its genesis and implications for the gold-mining industry, in: Petruk, W., Rule, W.A. (Ed.), Process Mineralogy XII: Applications to Environment, Precious Metal, Mineral Beneficiation, Pyrometallurgy, Coal and Refactories. The Minerals, Metals & Materials Society, Warrendale, PA, p. 10.

Vyalikh, A., Massiot, D., Scheler, U., 2009. Structural characterisation of aluminium layered double hydroxides by 27Al solid-state NMR. Solid State Nuclear Magnetic Resonance 36, 19-23.

Wang, D.-Y., Costa, F.R., Vyalikh, A., Leuteritz, A., Scheler, U., Jehnichen, D., Wagenknecht, U., Häussler, L., Heinrich, G., 2009. One-step synthesis of organic LDH and its comparison with regeneration and anion exchange method. Chemistry of Materals 21, 4490-4497.

Zheng, P., Chang, P.R., Ma, X., 2013. Preparation and characterization of rectorite gels. Industrial and Engineering Chemistry Research 52, 5066-5071.